Lab on a Chip

Accepted Manuscript

ROYAL SOCIETY OF CHEMISTRY

www.rsc.org/loc

A swallowable, capsular fluorometer simplifies detection of upper gastrointestinal bleeding by wirelessly detecting presence of fluorescein-spiked blood in the stomach.

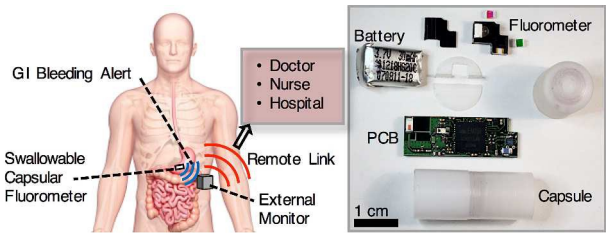

Lab on a Chip RSCPublishing

PAPER

Swallowable Fluorometric Capsule for Wireless Triage of Gastrointestinal Bleeding

Cite this: DOI: 10.1039/x0xx00000x

A. Nemiroski[a], M. Ryou[b], C.C. Thompson[b] and R.M. Westervelt[c,d]

Received 00th XX XXXX,
Accepted 00th XX XXXX

DOI: 10.1039/x0xx00000x

Real-time detection of gastrointestinal bleeding remains a major challenge because there does not yet exist a minimally invasive technology that can both i) monitor for blood from an active hemorrhage and ii) uniquely distinguish it from blood left over from an inactive hemorrhage. Such a device would be an important tool for clinical triage. One promising solution, which we have proposed previously, is to inject a fluorescent dye into the blood stream and to use it as a distinctive marker of active bleeding by monitoring leakage into the gastrointestinal tract with a wireless fluorometer. This paper reports, for the first time to our knowledge, the development of a swallowable, wireless capsule with a built-in fluorometer capable of detecting fluorescein in blood, and intended for monitoring gastrointestinal bleeding in the stomach. The embedded, compact fluorometer uses pinholes to define a microliter sensing volume and to eliminate bulky optical components. The proof-of-concept capsule integrates optics, low-noise analog sensing electronics, a microcontroller, battery, and low power Zigbee radio, all into a cylindrical package measuring 11 mm x 27 mm and weighing 10 g. Bench-top experiments demonstrate wireless fluorometry with a limit-of-detection of 20-nM aqueous fluorescein. This device represents a major step towards a technology that would enable simple, rapid detection of active gastrointestinal bleeding, a capability that would save precious time and resources and, ultimately, reduce complications in patients.

Introduction

Gastrointestinal bleeding (GIB)—a condition caused by peptic ulcer disease, esophageal varices, and other erosive conditions (e.g. esophagitis, gastritis, duodenitis)—is a major health-concern across the globe.[1-3] In the United States alone, 300,000 patients are hospitalized every year with upper GIB, of which up to 19% die from complications.[4,5] Re-bleeding, after hemostastatic treatment, occurs in up to 15% of patients within just five days,[6] and is strongly correlated with overall mortality.[7,8] Effective monitoring for re-bleeding in the hours and days after hemostasis remains problematic, especially in the early stages of blood loss (< 15% of total circulating blood volume) when physiological vital signs are not significantly affected. Common clinical options, such as monitoring vital signs, observation of clinical status (e.g. melena, hematemesis),[9] and serial hematocrit/hemoglobin checks, can be imprecise, and often require clinical interpretation.[10,11] Furthermore, these methods typically do not indicate a bleeding event in real time and sometimes call attention to a bleeding event only after significant blood loss.[12]

More advanced methods of detecting GIB, such as traditional endoscopy, capsular endoscopy,[13] angiography[14] and radionuclide scanning also suffer from several important limitations. Traditional endoscopy can detect minor GIB and can be used to differentiate between past and active GIB, but is expensive, time consuming, and cannot be used to monitor continuously over a long period of time. Wireless capsular endoscopy that uses video recording can monitor over ~24 hr and can be used to identify blood in the stomach, but cannot be used to reliably differentiate past and active GIB because evidence of blood in the stomach is not necessarily an indicator of active GIB. Furthermore, this method requires tedious expert analysis of many hours of recorded video. Angiography and radiolabeling are very accurate, but monitoring continuously over a period of hours or days is expensive and impractical. To our knowledge, there are no technologies currently capable of directly and uniquely detecting active GIB, or monitoring for future GIB over the course of hours to days. A new method to specifically detect early stage GIB, in real-time, could radically improve the treatment options for upper GIB patients.

We have previously described a new approach that can differentiate past vs. active GIB by introducing a fluorescent contrast agent, fluorescein, into the cardiovascular system through an intravenous injection.[15] If the patient suffers from active GIB—and only in that case—the fluorescent dye would enter the GI tract and be detected by a wireless fluorometer, which would ideally be small enough to be swallowed. Several fluorescence sensors have previously been developed by us and others for use in inside the body, but they have been either far too large to swallowed[15,16] or designed to remain tethered[17,18].

In this paper we report the construction of a miniaturized capsular fluorometer that is suitable for swallowing and designed specifically for identifying early-stage GIB. The fluorometer is integrated into 11 mm x 27 mm capsule with telemetry based on the commercial IEEE 802.15.4 Zigbee wireless protocol operating at 2.4 GHz.[19] For fluorescence detection, we employed a right-angled optical configuration that uses pinholes to eliminate the need for bulky focusing optics. Low noise detection electronics and on-chip digital filtering enabled submicromolar sensitivity despite a 0.2-μL sample volume and lack of focusing optics. We have designed the device to transmit data, in real-time, to a monitoring device that could be mounted

immediately outside the body. Figure 1 shows a schematic of the flow of data between the capsular fluorometer, the external monitor, and the local area network of a hospital, which would route data to the appropriate medical personnel.

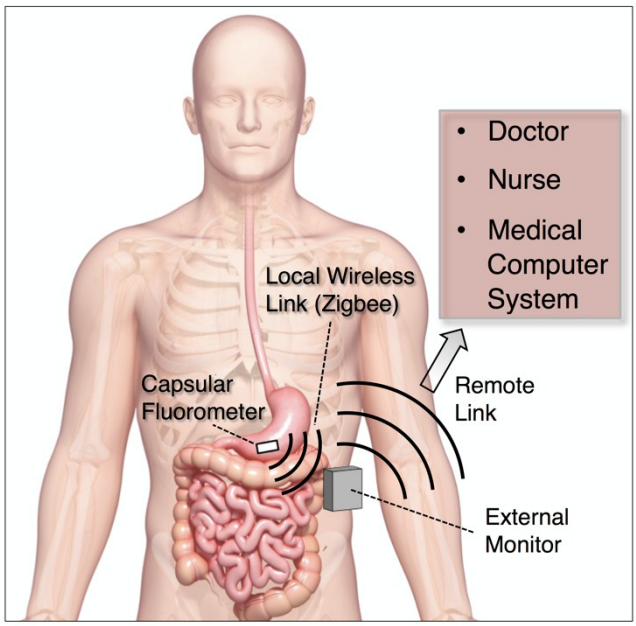

Fig. 1: Body Area Network that connects the swallowable capsular fluorometer to an external device through a Zigbee-based wireless connection.

Experimental Design

Capsular Construction and Packaging

Figure 2A shows a schematic of the capsular fluorometer. The heart of the device is a miniature (7 mm x 7 mm) system-on-chip (EM250, Ember) that includes a 12 MHz XAP2b 16-bit microcontroller core, 128 kB of flash memory, a 2.4 GHz Zigbee radio, and a 12-bit sigma-delta ADC. The ADC features a sample rate of 1.65kHz, a voltage range of 1.2 V, and a resolution of $\Delta v_{adc} = 1.2V / 2^{12}$ bits = 0.3 mV. Additional components include an antenna (WE-MCA, Wurth Electronics Inc.), a passive RF matching network, and various decoupling capacitors. For almost all passive components (resistors, capacitors, inductors), we used an 0402 package to minimize the footprint of the PCB. To prevent electrical coupling between the two analog circuit paths, we used separate 3.3-V voltage regulators to supply power to the photodiode amplifier and LED.

After assembling all surface-mount components onto a custom-designed, 4-layered, printed circuit board (PCB) manufactured by Advanced Circuits Inc, we adhered the assembled fluorometer to the PCB with epoxy and soldered the four leads (two each on the LED and photodiode) to the PCB with small wires. We then uploaded the Zigbee firmware and all custom software for data acquisition (DAQ) to the microcontroller. To reduce the device footprint, we permanently cut off the programming connector after completing the upload.

We soldered a 3.7-V Li-Polymer battery (LP30-FR, Plantraco) with a lifetime of $Q_{batt} = 30$ mAH to the assembled PCB. We next wrapped the entire device with a layer of insulating Kapton tape and a layer of aluminium foil grounded to the negative terminal of the battery to shield the device from external electromagnetic interference. Finally, we inserted the bundle into a machined, hollow Delrin cylinder (11 mm x 27 mm), sealed the optical side with epoxy, and affixed a Delrin end-cap to seal the capsule.

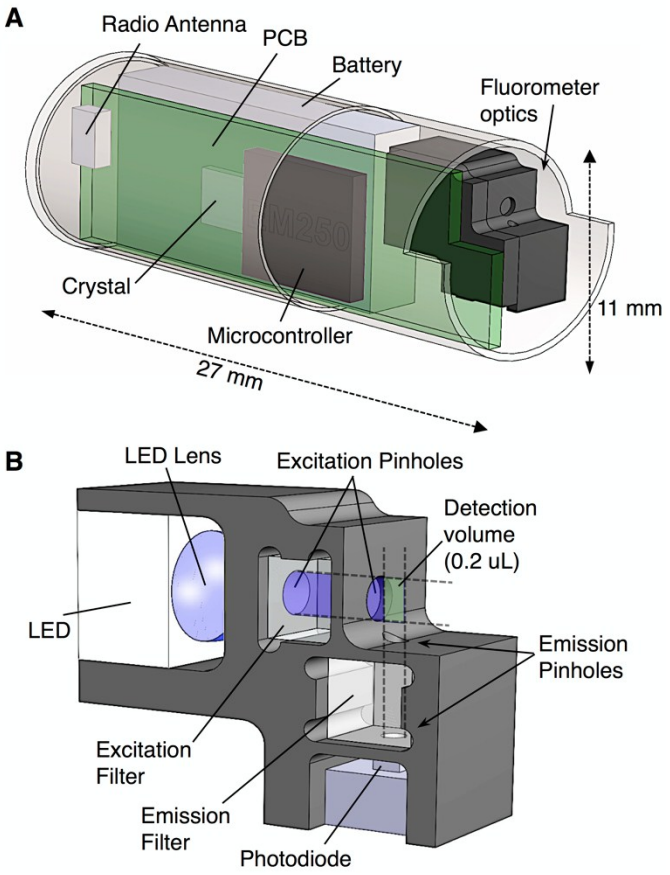

Fig. 2 Schematic of the components and housing of capsular device (A) the fluorometer components and optical paths (B).

Optoelectronic Design

Figure 2B shows a schematic of the optical front-end used to detect fluorescence. For excitation and detection, we used (i) a surface mount LED (LB E63C, Osram Inc.) with a peak wavelength of 465 nm and (ii) a silicon photodiode (PDB-C122, Advanced Photonix, Inc.). To ensure high illumination efficiency, we chose an LED that included an integrated lens that constrained the divergence angle of emitted light to 45˚. To filter the excitation and emission signals we used (i) a low pass excitation filter (NT64-593, Edmund Optics) with a cut off at 490 nm and a thickness of 1.6 mm and (ii) a band pass emission filter (MF525-39, Thorlabs) centered at 520 nm with a 40-nm full width at half maximum and a thickness of 1.9 mm. We cut the large optical filters into 2 x 2 mm^2 squares with a wafer-dicing saw.

We constructed a miniature housing for the optical components out of black Delrin acetel thermoplastic (DuPont) that we machined with a CNC mill using a 0.02" diameter, 2-flute square endmill (GR2SI0.02, Roundtool Labs). We chose Delrin due to the ease with which it can be machined, and its biocompatibility. A pair of 0.5-mm coaxial pinholes on both sides of the emission filter, and 1.0-mm coaxial pinholes on both sides of the excitation filter provided two functions: i) they eliminated coupling of the intense LED light into the photodiode and ii) they defined a 0.2-μL volume of detection at the intersection of

the optical paths of the excitation and detection optics. After inserting all four optical elements into the housing, we affixed a delrin cover piece with epoxy (BONDiT B-45TH, Reltek,US). The overall size of the fluorometer was 9.7 mm x 8.9 mm x 3.7 mm. We include a more detailed description of the characterization of the filters and construction of the fluorometer in the Supporting Information.

Spectral Characterization

We characterized the spectra of the LED, excitation filter, and emission filter within the optical housing using an optical fiber-coupled spectrophotometer (HR2000CG-UV-NIR, Ocean Optics Inc.) and white light source (100-W Mercury lamp, Chiu Tech. Corp.). To collect the transmission spectrum of the emission filter at non-normal angles of incidence, we used an uncut filter. We provide further details on this experimental set-up in the SI.

Signal Transduction and Data Acquisition

Figure 3 shows a schematic of the analog electronics used to transduce the optical signal. To convert the photodiode current to a voltage, we implemented a bootstrapped transimpedance amplifier (TIA) using a single opamp (AD4505, Analog Devices) with a feedback resistor R_f = 330 MΩ to yield a first-stage conversion gain of 0.33 mV/pA. A 1-pF capacitor in parallel with the feedback resistor eliminated ringing due to gain peaking and, together with the intrinsic roll off of the TIA, formed a low pass filter with a pole at 555 Hz. A second amplification stage, consisting of a 50X-inverting amplifier, yielded a final amplification of a_{iv} = 16.5 mV/pA at the input to the analog-to-digital converter (ADC). A 5-nF capacitor in parallel with the second stage formed an additional low pass filter with a single pole at 318 Hz to further suppress high frequency noise.

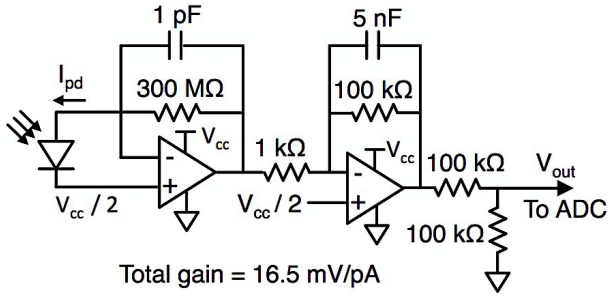

Fig. 3: Schematic of analog electronics for signal transduction

The two stages combined for an equivalent noise bandwidth Δf_{ENB} = 313 Hz, which was well below the Nyquist frequency f_n = 825 Hz (one-half of the 1.65-kHz sample rate) of the analog-to-digital converter. Within Δf_{ENB}, we measured an input referred current noise of i_{in} = 9 fA/$\sqrt{\text{Hz}}$, which primarily consisted of the Johnson noise due to the high R_f and photodiode shunt resistance R_s = 500 MΩ. The raw input-referred current resolution was $\Delta i_{raw} = \Delta v_{adc}/a_{iv}$ = 18 fA. To further reduce the influence of white noise and 1/f noise in the TIA (corner at 10 Hz), while staying within the range of the low-pass filters, we programmed the device to perform the following sequence (Fig. S1): i) pulse the LED at 92 Hz over N_{LED} = 40 cycles of the digital square wave, while sampling the ADC at 1.65 kHz (18 samples per pulse; N = 720 total samples), ii) multiply the acquired data by +1 when the LED was on and -1 when the LED was off, and iii) average all N samples together into a single data value. This sequence was essentially a digital version of a gated lock-in amplifier that narrowed the measurement bandwidth to $\Delta f = f_n/N$ = 1.15 Hz, centered on the signal, and also further improved the current resolution to $\Delta i = \Delta i_{raw}/\sqrt{N}$ = 0.7 fA.

Telemetry

After processing a value, the device sent the data over the onboard Zigbee radio to a remote Zigbee parent coordinator in the form of a USB dongle (ETRX2, Telegisis) connected to a personal computer running a custom program for DAQ implemented in MATLAB (Mathworks). We configured the device to establish a connection with the Zigbee parent immediately upon powering up. The device remained associated with the same parent until it is shut down. Once the network link was established, it entered a low quiescent current sleep cycle (I_{sleep} ~ 1 μA) until an event triggered the device to wake up and perform a function. We programmed the device to wake up, acquire data, store the extrapolated signal to memory, and send the processed data to remote Zigbee parent node with a duty cycle of 3 seconds. To remain associated with a Zigbee network, the device also polled the parent node with a duty cycle of 1.5 seconds. We include further details in Supporting Information.

Calibration of Fluorometer and Detection of Blood

We first prepared stock dilutions of aqueous fluorescein in the range of C = 0.01–1.0 mM. To characterize the performance of the device, we simulated the detection of GIB by i) initiating the device ii) fixing it with stationary clamp, and iii) submerging it in 200-mL beaker filled with 100 mL of deionized water. This system functioned as a simulated stomach with liquid contents. We rotated a magnetic stirring rod at 600 RPM at the bottom of the beaker to ensure rapid equilibration of any added sample. Next, we sent a wireless command to the capsular device to activate the DAQ process.

To calibrate the sensitivity of the device, we sequentially pipetted 1 mL of each aqueous stock solution (in order of increasing concentration) to the beaker. We streamed the data wirelessly to the Zigbee parent node connected to personal computer. To simulate GIB, we first prepared a 17.2 μM solution of fluorescein in whole blood by adding 0.1 mL of the 1-mM aqueous stock solution of fluorescein to 5.8 mL of heparinized porcine whole blood (Farm to Pharm LLC.). To simulate a bleeding event, we injected 1-mL of the blood/fluorescein mixture into a beaker with 100 mL of deionized water, yielding a simulated concentration of fluorescein in the stomach of C_s = 170 nM. We include further details about the experimental setup in the Supporting Information.

Results and Discussion

Model for Fluorescein as a Proxy for Acute GIB

Target Specification. We designed the device to be able to detect early GIB, which would be any lost volume of blood $V_b < 0.15V_T$, where V_T is the total volume of blood in the circulatory system ($V_T \approx$ 5 L for an adult human male). We therefore require a threshold bleed volume $V_a << 750$ mL to remain well within this boundary. We do not, however, want to be sensitive to ultra-small bleed volumes, which may not be indicative of a problem, and thus we choose a threshold bleed volume of V_a = 10 mL. We focus our detection on the stomach, which behaves as a collection point for fluids and is the most capacious

segment of the GI tract. For equivalent cumulative volume V_b of blood loss in any part of the GI tract, the lowest concentrations of tracer will be attained in the stomach. The detector must, therefore, be able to detect a cumulative volume of blood loss in the stomach $V_b \geq V_a$. Because the emptying of the stomach occurs within four hours,[20] we specify that the device must be able to detect V_a of blood within this time span.

Pharmacokinetic and Optical Properties of Fluorescein. We chose fluorescein as a proxy for active GIB because it is commonly used, is approved for use *in vivo* by the U.S. Food and Drug Administration (e.g., in opthomalogy), has a high fluorescence quantum yield (~90%), and has an optical spectrum (absorption peak at 494 nm; emission peak at 512 nm)[21] that does not overlap with the autofluorescence spectrum of gastric juice (absorption peak at 288 nm; emission peak at 350 nm)[22-24]. The isolation of the absorption and emission peaks of fluorescein from the native background of the stomach enables fluorescein to serve as a unique marker for blood as a foreign substance in the stomach.

A typically used dosage for an adult male delivers 500 mg of fluorescein disodium (332.3 g/mol) into ~5 L of blood for an initial intravenous concentration $C_0 \sim 300$ μM.[25] Any foreign substance introduced into the cardiovascular system will not remain in the blood stream indefinitely. The pharmacokinetic properties of fluorescein, in particular, are dictated by several complex pathways, which include: i) filtration by the kidneys, ii) absorption by or diffusion through the walls of the blood-vessels, or iii) chemical conjugation into fluorescein glucuronide, which has suppressed fluorescence.[26,27] The time dependant effective concentration of fluorescein $C_{iv}(t)$ after initial intravenous injection in humans has been reported previously by Blair *et. al.*[28] Based on these data, we constructed Table 1, which summarizes the equivalent intravenous fluorescein concentrations after an initial injection with concentration C_0.

Table 1: (Central column) Typical intravenous elimination of fluorescein from blood in an adult human male, extrapolated from Blair et al.[28] (Right column) The equivalent concentration of fluorescein in the stomach $C_S(t)$ that would undergo a 1:100 dilution, which we define as the worst-case scenario. The shaded data represents the typical time of gastric emptying; the bolded data represents the limit of detection of our device, under the assumptions of our simple model for GIB.

t (hr)	$C_{iv}(t)$ (μM)	$C_S(t)$ (nM)
0	300	3000
0.5	60.6	600
1	32.8	325
2	17.2	170
4	5.6	55
6	2.8	28
7.5	**2.0**	**20**
12	0.9	9
24	0.3	3

Bleeding Model. We develop a simple model for linking the detected concentration of the tracer in the stomach to V_b, the cumulative volume of leaked blood. We define the detection of GIB as a binary test with threshold volume V_a: the device must be able to detect bleeding for which $V_b > V_a$. In practice, our approach will be bound by the limit-of-detection (LOD) of the fluorometer, the lowest concentration C_{LOD} of fluorophore that it can detect.

Figure 4 shows the parameters used in this model. We make the following assumptions to simplify the analysis: (i) there is an initial volume V_0 of fluid already present in the stomach at $t = 0$; (ii) this fluid is primarily aqueous because the patient would have consumed ~1L of water prior to the intravenous administration of fluorescein; (iii) the sensor is submerged in the fluid within the stomach with a volume $V_s(t) = V_0 + V_b(t)$ and measures the concentration C_s of tracer at time $t > 0$; (iv) any tracer that enters the stomach instantly diffuses to equilibrium, such that $C_s(t)$ is spatially homogenous. If V_b was injected instantaneously at $t = \tau$, it would deliver less fluorophore into the stomach than if it bleed out in any other way during $0 < t < \tau$ because the intravenous concentration $C_{iv}(t)$ is monotonically decreasing. If any part of V_b leaked earlier, it would have delivered more fluorophore into the stomach and would therefore attain a higher C_s (we include a proof in the SI). To detect GI bleeding, we must be able to detect at least $V_b = V_a$ of blood loss. We find that the minimum possible concentration C_a that could correspond to the threshold V_a is

$$C_a(\tau) = \left(\frac{V_a}{V_0+V_a}\right) C_{iv}(\tau). \quad (1)$$

Under these assumptions, if $C_{LOD} \geq C_a$, then the fluorometer can detect any type of bleed $V_b \geq V_a$ during the time $0 < t \leq \tau$. Ultimately, when $C_a(\tau) < C_{LOD}$, we can no longer be certain that we can detect V_a.

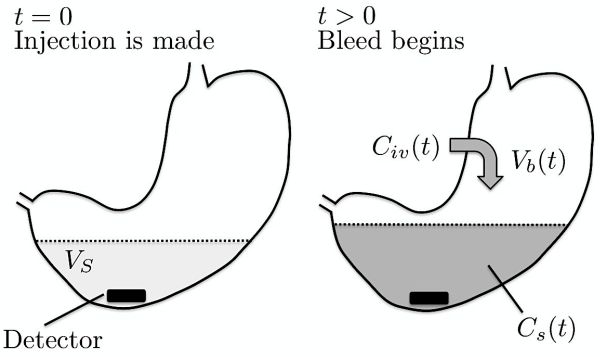

Fig.4: Gastrointestinal bleeding model

Design and Performance of Capsular Fluorometer

Overview. The final capsular device weighted 10 g and the bill of materials (BOM) for low volume purchase (~10 of each component) was $110 (SI); if purchased in bulk (>10^3) components at a time, the BOM could be reduced to significantly (< $30). Figure 5 shows the assembly of the capsular fluorometer.

Optical Pinholes. The primary challenge to the miniaturization of a fluorometer is to control the angle of incidence between the light and the optical filters without resorting to bulky optical components. To eliminate background from the excitation source, we require excellent isolation between the close excitation and emission peaks of fluorescein (the peak wavelengths are ~30 nm apart). Interference filters provide the sharpest cut offs and highest attenuation outside the pass band and, for this reason, are most commonly used in fluorescence microscopy. The passband properties of interference filters are optimized for light at normal incidence; light that is incident at an angle from the normal will experience a shifted or broadened passband because of the angle dependant periodicity of the stacked dielectric films found in an interference filter. In standard fluorescence microscopy, focusing and collimation optics ensure that the excitation and emission are always at normal incidence with respect to the optical filters. In designing a miniature, integrat-

ed fluorometer, we do not have the luxury of space to satisfy this condition.

We can, however, constrain the allowed angles by using an appropriate set of pinholes, which are very low profile. As expected, we found that both filters exhibited a blue shift in their pass bands with increasing angle of incidence. Figure 6 shows the angle constrained by the emission pinholes and the measured shift in the passband of emission filter at the maximally allowed angle of angle 17˚. We found that with this geometry, the cut-on of the emission filter only shifted to shorter wavelengths by at most ~ 5 nm. We include further details in Supporting Information.

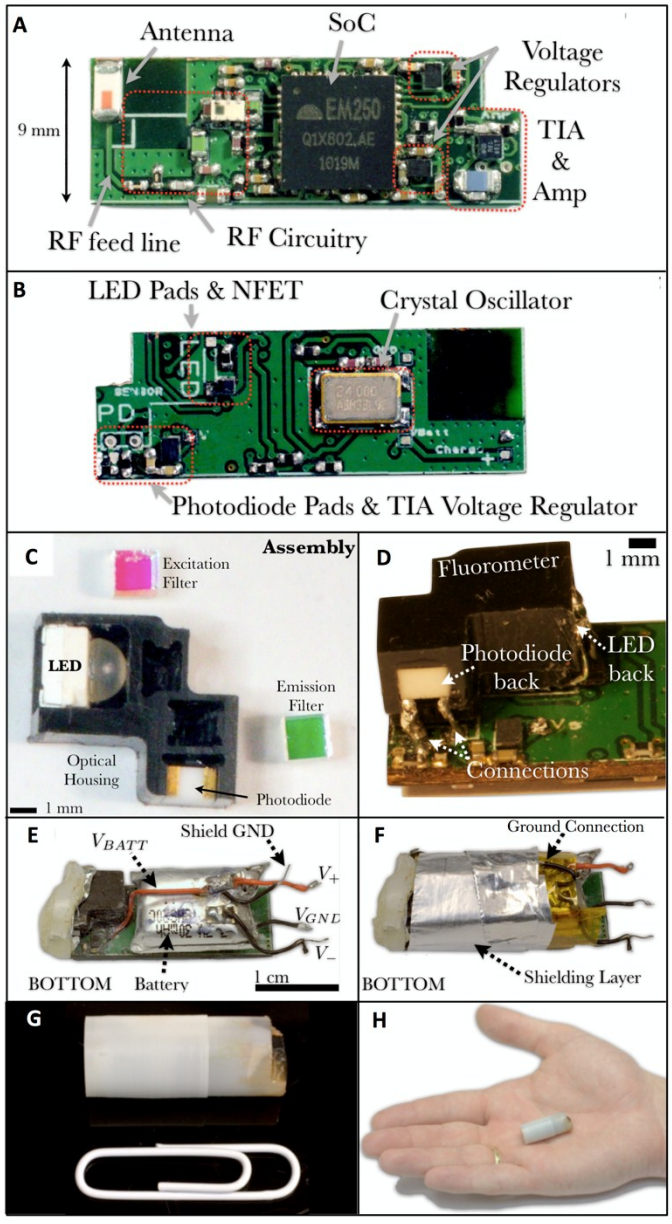

Fig 5: Photographs of the capsular fluorometer. (A-B) Top and bottom of the assembled 4-layer PCB that houses all electronic components. (C) Optical components and optical housing of the fluorometer. (D) Mounting of assembled optical sensor onto the PCB. (E) Complete device without encapsulation. (F) Device with electromagnetic shielding. Encapsulated fluorometer pictured next to a standard paperclip (G) and in the palm of a hand (H).

Signal Transduction. In the detection of analog signals, there exists an inherent trade-off between gain, noise, component count, current consumption, and voltage supply. To achieve low limits of detection, it is preferable to use very low-noise components with high gain, a goal typically reached with several stages of amplification and filtering powered by a well grounded power supply that runs on wide positive and negative voltage rails (e.g. ± 15 V).

In a swallowable capsule, however, there are three important constraints: i) all electronics must run off a single-sided, low voltage supply (e.g. ~3 V) to be compatible with standard battery technology (e.g. Lithium Ion, Lithium Polymer, Alkaline); ii) the number of components should be as low as possible to preserve space and power; and iii) the design should use off-the-shelf components that are inexpensive so that the device is disposable (as is necessary for *in vivo* applications)

Here, we have endeavoured to optimize the circuit design with respect to these constraints, while achieving low-noise operation (i_{in} = 9 fA/$\sqrt{\text{Hz}}$), and high gain (16.5 mV/pA) using only two stages of amplification. We also implemented a 720-point digital lock-in filter to reduce the measurement bandwidth to Δf = 1.15 Hz and supress noise even further. After performing this sequence, we measured the root-mean-square, input-referred noise to be $I_{in} = i_{in}\Delta f$ = 10 fA_{rms}. The limit of detection of the signal current was therefore $I_{LOD} = 3I_{in}$ = 30 fA, at the noise floor. Using the responsivity of the photodiode (R = 0.27 A/W; specified in the datasheet supplied by the manufacturer), we estimate that the limit of detection of optical power was $P_{LOD} = I_{LOD} / R$ = 110 fW. We include further details in the Supporting Information.

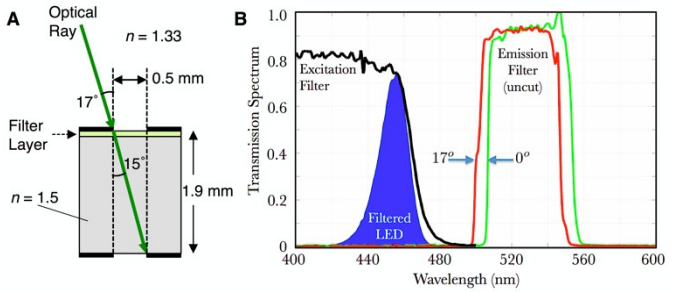

Fig. 6: Angles of incidence of the emission filter. (A) Maximum angle of incidence (17˚) defined by 0.5-mm pinholes separated by a 1.9-mm filter. (B) Spectrum of the excitation filter, filtered spectrum of the excitation LED, and spectra of the emission filter at normal incidence and 17˚ from normal.

Battery Lifetime and Wireless Communication

To determine the current consumption we measured the voltage drop across a 5Ω-resistor placed in series with the battery during each stage of operation. We found that each instance of DAQ typically consumed Q_{DAQ} = 0.58 mC + N_{LED} x 0.14 mC. The radio transmission of a single packet of data typically consumed Q_{TX} = 0.58 mC + N_{TX} x 0.07 mC, where N_{TX} is the number of 16-bit integers transmitted (typically we only send one at a time). Polling consumed a fixed Q_{poll} = 0.54 mC per poll. The lifetime of the battery is therefore

$$L = \frac{Q_{batt}}{Q_{DAQ}f_{DAQ}+Q_{TX}f_{TX}+Q_{poll}f_{poll}+I_{sleep}}, \qquad (2)$$

where f_{DAQ}, f_{TX}, and f_{POLL} are the repetition rates for DAQ, transmission of data, and polling of the network, respectively,

and Q_{batt} is the total charge of fully charged battery. For the basic settings that we implemented, $f_{POLL} = 0.67$ Hz which limits the maximum lifetime to L = 3.5 days. We acquire and transmit a single value (N_{TX} = 1, N_{LED} = 40) every 3 seconds ($f_{DAQ} = f_{TX} = 0.33$ Hz), to yield a total lifetime of L = 1.7 days. If the measurement and transmission duty cycle were increased to 5 minutes ($f_{DAQ} = f_{TX} = 3.3$ mHz), the battery could last for L = 3.3 days on a single charge.

In principle, the device can be set to poll the network and send data only if bleeding is detected. In this case, the average current consumed during DAQ is comparable to the sleep current, and the device could continue making measurements every 5 minutes for $L \sim 1.2$ years. This lifetime is unnecessary for swallowable gastrointestinal probes, but maybe useful for chronic, anchored probes or sub dermal implants.

Although the IEEE 802.15.4 standard at 2.4 GHz was originally intended for multi-sensor networking indoors, it can also be used for body network sensing for implantable and swallowable devices. Valdastri *et. al.*[29] has demonstrated that this wireless protocol has sufficient power and capacity for error correction to sustain a robust wireless link between a device inside the GI tract of a large pig (which is an animal commonly used model the human body in medical studies) and a small external receiving unit within ~ 1 m of the animal. We have also verified this capability in our previous work.[15]

Calibration of the Fluorometer and Detection of Simulated GIB

Figure 7A shows calibration series performed with the capsular fluorometer in aqueous solutions of fluorescein. We found that a least-squares fit to the response was linear ($R^2 = 0.995$) with a sensitivity S = 1.5 fA/nM. The concentration limit of detection C_{LOD} of aqueous fluorescein is related to the noise floor of the device (*i.e.*, the signal with no added fluorescein; shown on the left side of Figure 7B) by $C_{LOD} = I_{LOD} / S$ = 20 nM. To achieve this low-noise operation, we performed digital signal averaging over Δt_0 = 0.44 s (N = 720 samples acquired at 1.65 kHz). Using the experimentally found C_{LOD} for our chosen Δt_0, we can estimate the concentration LOD at any other averaging time Δt by $C_{LOD}(\Delta t) = 20\text{ nM} \cdot \sqrt{\Delta t_0 / \Delta t}$. When necessary, a lower C_{LOD} may be achieved by increasing the averaging time Δt; by contrast, faster operation may be achieved at the expense of increased C_{LOD}. Our choice of Δt_0 reflects a suitable compromise between fast operation (we only need to perform a measurement, at most, once every few seconds) and an acceptable limit of detection (we need C_{LOD} < 55 nm; as shown in Table 1). We include further details in the Experimental Design section and in the Supporting Information.

To simulate GIB occurring within the gastric emptying time, we chose a time point of τ = 2 hr after a hypothetical intravenous injection of C_0 = 300 μM. Using Table 1, we find that this time, the typical intravenous concentration of fluorescein would be C_{iv} = 17.2 μM. If, at this time, V_a = 10 mL of blood leaks into the stomach with V_0 = 1 L of water already present, the fluorescein would be diluted to C_s = 170 nM. To simulate this event, we prepared whole blood with C_{iv} = 17.2 μM of fluorescein.

Figure 7B shows the time trace of the measured current that the device transmitted wirelessly during injection of 1 mL of this fluorescein/blood mixture into 100-mL of aqueous solution. We continued acquiring data until the signal stabilized following the introduction of the blood/fluorescein mixture. The signal reached a steady state after ~2 minutes. At that point, we averaged the measured current over n = 20 consecutive periods for a steady state current of I = 252 fA, which corresponded to a measured concentration of $C = I/S \pm C_{LOD}/\sqrt{n}$ = 168 ± 4 nM, matching the expected concentration of 170 nM. When we set the threshold of detecting a bleeding event to be at I_{LOD} = 30 fA, the detection was triggered ~9 s (3 periods of measurement) after the injection the blood/fluorescein bolus.

In our model for GIB we defined a typical worst-case scenario as 10 mL of blood injected into the stomach that already has 1 L of water present. Whatever the C_{iv} is at the time of the bleed, in this case, it will be diluted by 1:100 in the stomach. If there is less the 1 L of water in the stomach, the fluorescein will be less dilute, leading to a higher signal. Because there are many ways to achieve the same concentration of fluorescein, we define detection simply as a signal that passes the worst-case threshold, defined in the rightmost column of Table 1. Under these general assumptions, and given the experimentally determined C_{LOD} = 20 nM, the fluorometer has sufficient sensitivity to detect > 10-mL of blood leaked into the stomach, over the course of ~7.5 hr after fluorescein injection (well beyond the typical gastric emptying time of ~4 hr). In principle the device can detect well beyond that, along the entire GI tract, where the dilutions are likely to be less than in the stomach. If less water is present in the stomach, than this time will be extended as well. For example, if we define a worst cast bleed as undergoing a 1:10 dilution, then the device could detect a bleed volume V_a for up to ~24 hr.

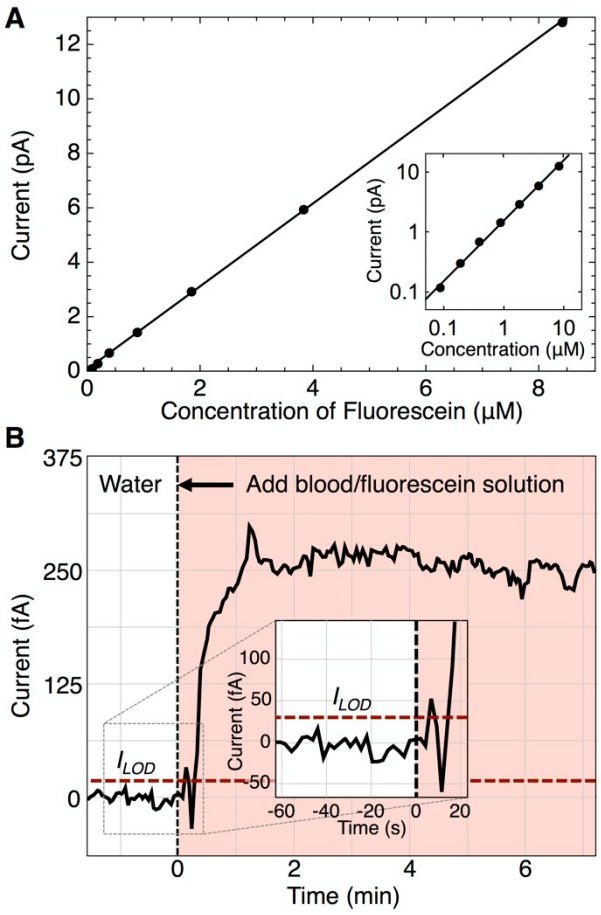

Fig 7: Calibration of fluorometer and detection of blood. (a) Fluorometer current vs. concentration of fluorescein in water (slope = 1.5 pA/μM, R^2 = 0.9998). Inset: Logarithmic representation of concentration vs. current (slope = 1.0, R^2 = 0.9977). (b) Time trace of fluorometer current vs. time during the detection of 1-mL blood/fluorescein mixture added to 100-mL of water at time t = 0.

Conclusion

In this paper, we have described the development of a fluorometer that i) is small enough to be integrated into a swallowable capsule, ii) can perform highly sensitive fluorescent detection in a liquid medium, iii) can transmit results of testing wirelessly, and iv) can identify active GIB as uniquely different than blood accumulated from past GIB. By using small pinholes and interference filters, we have minimized the size of the fluorometer. The open-to-the-environment design enables fluorescence to be detected from liquid external to the capsule and reduces the chance that the contents within the GI tract would clog the optics. Our design enabled us to detect very weak optical signals (P_{LOD} = 110 fW), and low concentrations of fluorescein (C_{LOD} = 20 nM), which in term will enable the detection of low volumes of blood in the GI tract. Using a single, low-power system-on-chip enabled the ADC, microcontroller, and radio to be integrated into a single, compact package with minimal footprint. Using almost exclusively off-the-shelf components ensured that the device was inexpensive enough (BOM < $110) to be disposable, as it would have to be for single use.

The primary use of this technology would be as a tool for clinical triage via rapid detection of active GIB in the stomach. In this application, the patient would already have fasted to clear the stomach of any contents and would consume ~1 L of water before administration of intravenous fluorescein to i) dilute any fluorescein-spiked blood that enters the stomach and ii) neutralize the pH of the stomach fluid.

Applications that require extended use (*i.e.*, days to weeks) of the capsular fluorometer in the stomach may present challenges that may be overcome by additional modifications to the device. For example, as the acidity of the stomach gradually returns to pH 1.5 several hours after the patient has ingested water, the spectral properties of fluorescein will change because they are known to depend on pH. As the pH is decreased from neutral, the excitation peak of fluorescein shifts gradually towards λ = 435 nm and the overall quantum yield can decrease by a factor as low as ~0.25x.[30] Strategies to compensate for the overall reduction in signal may include i) increasing the power of the excitation source and/or adding a second light source (or use of a dual-wavelength LED or laser) with peak wavelength around λ = 435 nm to guarantee sufficient excitation, even at low pH, and ii) increasing the integration time Δt to increase the signal-to-noise ratio of the detection electronics. Another potential challenge to long-term usage is gastric emptying. To circumvent gastric emptying at times beyond ~4 hr, it may be possible to fix the capsular fluorometer semi-permanently to the mucosa by an endoscopic clip. For applications that require usage of the device beyond the stomach, it may be necessary to detect the position of device at all times during its transit through the GI tract (e.g., to locate the source of GIB). Using additional, external RF sensors could enable the position of the capsule to be tracked by triangulation based on signal strength.[31] The addition of a small magnet could also enable precise tracking in 3D space by an externally worn array of magnetic sensors.[32] The addition of a pH and/or temperature sensor could also provide information about GI motility.[33]

Future work will entail *in vivo* verification of the device in an animal study with simulated GIB, similar to our previous work with larger sensors.[15] Further miniaturization of the capsular fluorometer (e.g., through integration of all electronics onto a custom integrated circuit, using a smaller battery, and using a laser-based excitation source to eliminate the lens and excitation filter) could enable delivery of the device to a specific location in the GI tract through the instrument channel of an endoscope. For clinical uses, it will likely be necessary to coat the device with a transparent, biocompatible polymer that is resistant to acidic corrosion, such as Parylene-C.

The miniature fluorometer we describe can also find applications in lab on chip applications that require miniaturized integration of fluorescence detection with microfluidics. With minor modifications, this device could also be adapted into a small hand-held reader for fluorescent detection of labelled biomolecules on paper-based test strips, or as a peripheral attachment to a smartphone for point-of-care applications.

Acknowledgements

This work was supported by the Harvard Nanoscale Science and Engineering Center (NSEC) under award# NSF/PHY 06-46094 and by the MIT-Harvard Center for Cancer Nanotechnology Excellence (CCNE) under award# 1U54-CA119349. We thank Jim MacArthur and Keith Brown for helpful discussions.

Notes and references

[a] Department of Chemistry and Chemical Biology, Harvard University, 12 Oxford St., Cambridge, MA 02138, USA. Email: anemiroski@gmwgroup.harvard.edu
[b] Division of Gastroenterology, Brigham & Women's Hospital, 75 Francis Street, Boston, MA 02115, USA.
[c] John A. Paulson School of Engineering and Applied Sciences, Harvard University, 9 Oxford St., Cambridge, MA 02138, USA.
[d] Department of Physics, Harvard University, 9 Oxford St., Cambridge, MA 02138, USA.

† Electronic Supplementary Information (ESI) available: [details of any supplementary information available should be included here]. See DOI: 10.1039/b000000x/

1 F. E. Silverstein, D. A. Gilbert, F. J. Tedesco, N. K. Buenger and J. Persing, *Gastrointestinal Endoscopy*, 1981, **27**, 94–102.
2 R. T. Yavorski, R. K. Wong, C. Maydonovitch, L. S. Battin, A. Furnia and D. E. Amundson, *Am. J. Gastroenterol.*, 1995, **90**, 568–573.
3 M. E. van Leerdam, *Best Pract Res Clin Gastroenterol*, 2008, **22**, 209–224.
4 M. E. van Leerdam, E. M. Vreeburg, E. A. J. Rauws, A. A. M. Geraedts, J. G. P. Tijssen, J. B. Reitsma and G. N. J. Tytgat, *Am. J. Gastroenterol.*, 2003, **98**, 1494–1499.
5 F. Fein, A. Weber, S. Koch, N. Festou, A. C. Dupont-Gossard, J. P. Cervoni, E. Monnet, M. Bardou and F. Carbonnel, *European Journal of Gastroenterology & Hepatology*, 2010, **22**, 361–367.
6 K. Bambha, W. R. Kim, R. Pedersen, J. P. Bida, W. K. Kremers and P. S. Kamath, *Gut*, 2008, **57**, 814–820.
7 P. W. Chiu, E. K. Ng, F. K. Cheung, F. K. Chan, W. K. Leung, J. C. Wu, V. W. Wong, M. Y. Yung, K. Tsoi, J. Y. Lau, J. J. Sung and S. S. Chung, *Clin Gastroenterol Hepatol*, 2009, **7**, 311–316.
8 S.-W. Lee, T.-Y. Lee and C.-S. Chang, *Dig. Dis. Sci.*, 2009, **54**, 1128–1134.
9 T. O. G. Kovacs, *Curr Gastroenterol Rep*, 2008, **10**, 535–542.
10 A. Languasco, L. Agustin, N. Cazap, C. Nicolas, S. Marciano, M. Sebastian, M. Huber, H. Marina, A. Novillo, N. Abel, F. Poletta, P. Fernando, M. Milberg, M. Matias, D. Riveros and R. Dardo, *J Hosp Med*, 2010, **5**, 283–288.
11 J. DePriest, *South Med J*, 1996, **89**, 386–390.
12 F. K. Cheung and J. Y. Lau, *Gastroenterol Clin North Am*, 2009, **38**, 231–243.
13 C. Hassan, A. Zullo, S. Winn and S. Morini, *Endoscopy*, 2008, **40**, 414–421.
14 C. J. Laing, T. Tobias, D. I. Rosenblum, W. L. Banker, L. Tseng and S. W. Tamarkin, *Radiographics*, 2007, **27**, 1055–1070.
15 M. Ryou, A. Nemiroski, D. Azagury, S. N. Shaikh, M. B. Ryan, R. M. Westervelt and C. C. Thompson, *Gastrointestinal Endoscopy*, 2011, **74**, 189–194.e1.
16 P. Valdastri, E. Susilo, T. Förster, C. Strohhöfer, A. Menciassi and P. Dario, *IEEE Trans. Biomed. Eng.*, 2011, **58**, 1846–1854.
17 K. K. Ghosh, L. D. Burns, E. D. Cocker, A. Nimmerjahn, Y. Ziv, A. El

Gamal and M. J. Schnitzer, *Nat. Methods*, 2011, **8**, 871–U147.
18 T. D. O'Sullivan, R. T. Heitz, N. Parashurama, D. B. Barkin, B. A. Wooley, S. S. Gambhir, J. S. Harris and O. Levi, *Biomed Opt Express*, 2013, **4**, 1332–1341.
19 G.-Z. Yang, Ed., *Body Sensor Networks*, Springer Science & Business Media, 2007.
20 M. Camilleri, L. J. Colemont, S. F. Phillips, M. L. Brown, G. M. Thomforde, N. Chapman and A. R. Zinsmeister, *Am J Physiol*, 1989, **257**, G284–G290.
21 R. Sjöback, J. Nygren and M. Kubista, *Spectrochim. Acta A*, 1995, **51**, L7–L21.
22 L. Y. Zhou, S. R. Lin, Y. Li, Q. M. Geng, S. G. Ding, L. M. Meng, X. N. Sun, J. T. Wang, Z. J. XU, H. L. Guo, C. G. LI and R. L. Cui, *J. Dig. Dis.*, 2011, **12**, 279–285.
23 W. Lian, D. J. Ma, X. Xu, Y. Chen and Y. L. Wu, *J. Dig. Dis.*, 2012, **13**, 100–106.
24 K. Deng, L. Y. Zhou, S. R. Lin, Y. Li, M. Chen, Q. M. Geng and Y. W. Li, *J. Dig. Dis.*, 2013, **14**, 299–304.
25 M. D. Douglas J Rhee, C. J. Rapuano and C. A. Weisbecker, *Ophthalmic Medicines 2003*, Physician's Desk Reference (PDR), 2002.
26 L. E. Tan, W. Orilla, P. M. Hughes, S. Tsai, J. A. Burke and C. G. Wilson, *Invest Ophthalmol Vis Sci*, 2011, **52**, 1111–1118.
27 D. Grotte, V. Mattox and R. Brubaker, *Exp. Eye Res.*, 1985, **40**, 23–33.
28 N. P. Blair, M. A. Evans, T. S. Lesar and R. C. Zeimer, *Invest Ophthalmol Vis Sci*, 1986, **27**, 1107–1114.
29 P. Valdastri, A. Menciassi and P. Dario, *IEEE Trans. Biomed. Eng.*, 2008, **55**, 1705–1710.
30 M. M. Martin and L. Lindqvist, *J. Lumin.*, 1975, **10**, 381–390.
31 A. Moglia, A. Menciassi, M. O. Schurr and P. Dario, *Biomed. Microdevices.*, 2006, **9**, 235–243.
32 C. Hedsund, I. Moeller Joensson, T. Gregersen, L. Fynne, V. Schlageter and K. Krogh, *Clin. Exp. Gastroenter.*, 2013, **6**, 201–208.
33 K. Tran, R. Brun and B. Kuo, *Therap. Adv. Gastroenterol.*, 2012, **5**, 249–260.

